ACSNANO

www.acsnano.org

ARTICLE

Efficient Genome Editing Achieved via Plug-and-Play Adenovirus Piggyback Transport of Cas9/gRNA Complex on Viral Capsid Surface

Zhi Hong Lu, Jie Li, Igor P. Dmitriev, Elena A. Kashentseva, and David T. Curiel*

Cite This: *ACS Nano* 2022, 16, 10443–10455

Read Online

ACCESS | Metrics & More | Article Recommendations | Supporting Information

ABSTRACT: **The capacity to efficiently deliver the gene-editing enzyme complex to target cells is favored over other forms of gene delivery as it offers one-time hit-and-run gene editing, thus improving precision and safety and reducing potential immunogenicity against edited cells in clinical applications. Here we performed a proof-of-mechanism study and demonstrated that a simian adenoviral vector for DNA delivery can be repurposed as a robust intracellular delivery platform for a functional Cas9/guide RNA (gRNA) complex to recipient cells. In this system, the clinically relevant adenovirus was genetically engineered with a plug-and-display technology based on SpyTag003/SpyCatcher003 coupling chemistry. Under physiological conditions, an off-the-shelf mixture of viral vector with SpyTag003 incorporated into surface capsid proteins and Cas9 fused with SpyCatcher003 led to a rapid titration reaction yielding adenovirus carrying Cas9SpyCatcher003 on the virus surface. The Cas9 fusion protein-conjugated viruses in the presence of a reporter gRNA delivered gene-editing functions to cells with an efficiency comparable to that of a commercial CRISPR/Cas9 transfection reagent. Our data fully validate the adenoviral "piggyback" approach to deliver an intracellularly acting enzyme cargo and, thus, warrant the prospect of engineering tissue-targeted adenovirus carrying Cas9/gRNA for *in vivo* gene editing.**

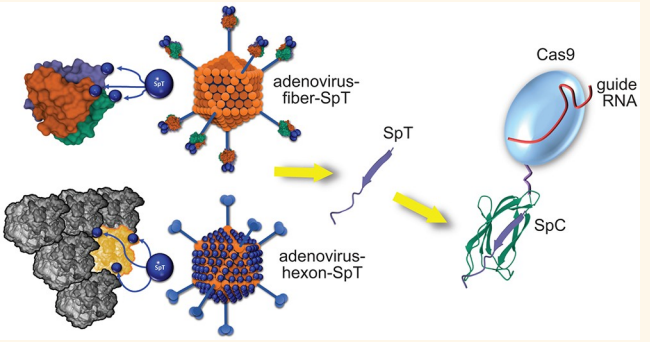

KEYWORDS: *simian adenovirus, Cas9/gRNA complex, gene editing, SpyTag003, SpyCatcher003*

The recent advent of a group of genetic manipulation enzymes, the clustered regularly interspaced short palindromic repeats (CRISPR)-associated protein (Cas) systems, represents a revolutionary advancement in the technology of precise and versatile gene editing and holds the promise of treating a great variety of inherited and acquired diseases.[1−5] The mainstay of Cas-mediated gene-editing strategies relies on introducing DNA sequences encoding an editor and guide RNA (gRNA) to the nucleus of target cells via viral or nonviral methods.[6−8] The DNA delivery, however, runs the risk of insertional mutagenesis by some of the viral vector systems and plasmid DNA.[9,10] Such DNA methods also result in production of Cas protein long after the on-target editing events are achieved; the undesired persistent Cas expression potentially increases off-target editing events and elicits a host adaptive immune response attacking the edited cells.[11] The recently emerging mRNA delivery systems allow transient expression of editors, thus circumventing the concerns of the DNA approach.[12,13] However, delivery of mRNA has the limitations of triggering innate immunogenicity against cells uptaking exogenous mRNA and susceptibility of mRNA to enzymatic degradation in blood and the periphery.[14] In this regard, protein-based formulations also offer one-time hit-and-run gene editing but, unlike mRNA, have a far smaller tendency of inducing an acute immune response, thus conferring improved specificity and enhanced safety over nucleic acid approaches.[15,16]

In this regard, Cas is a gRNA sequence-dependent DNA endonuclease, and purified Cas can directly bind *in vitro*-transcribed or synthesized gRNA to form the active ribonucleoprotein (RNP) enzyme complex. Exogenous Cas RNP complex, however, like many other intracellularly acting

Received: January 26, 2022
Accepted: May 25, 2022
Published: June 24, 2022

https://doi.org/10.1021/acsnano.2c00909
ACS Nano 2022, 16, 10443−10455

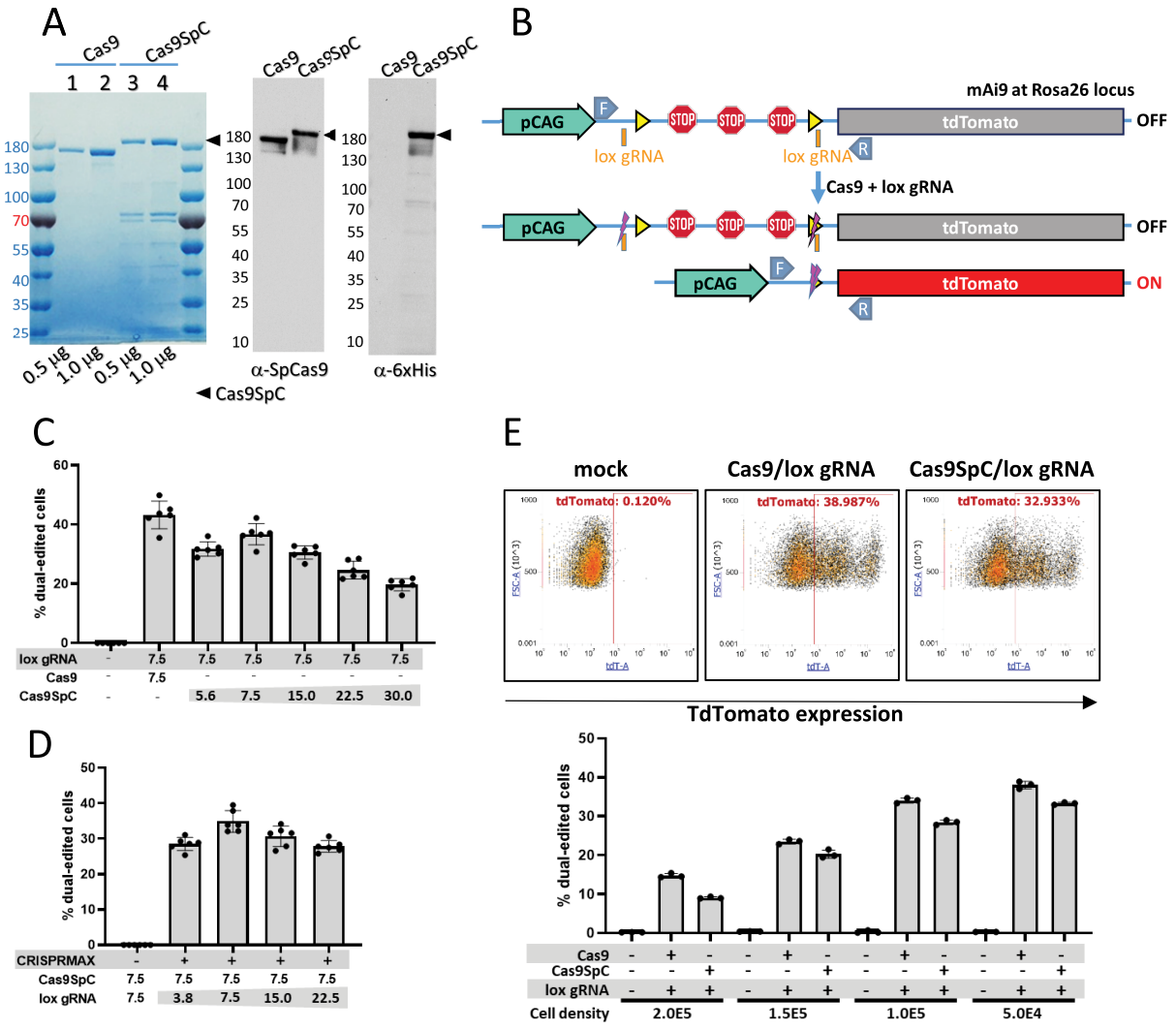

Figure 1. Cas9SpC retained CRISPR nuclease activity. (A) Cas9 and Cas9SpC with the indicated amounts were resolved on an SDS-PAGE gel followed by Coomassie blue staining (left) or by immunoblotting with anti-SpCas9 and anti-6xHis antibodies (middle and right). (B) Schematic diagram of the *Rosa26:Ai9-SauSpyCas9-tdTomato* (mAi9) locus without or with gene editing. Three SV40 polyadenylation signals (STOP) function as a potent transcription inhibition element to the downstream *tdTomato* gene. Endonuclease cleavage at both upstream and downstream sites by Cas9/lox gRNA can lead to a subset of alleles with deletion of the STOP cassette and activation of the *tdTomato* gene expression. The locations of duplicate lox gRNA sites and PCR genotyping primers are illustrated. (C and D) Scatter plots with a bar graph showing the percentage of tdTomato-positive cells by fluorescence microscopy analysis of mAi9 cells on day 4 following lipofectamine CRISPRMAX transfection with Cas9/lox gRNA or with Cas9SpC/lox gRNA. The numbers below the graphs indicate the amount of reagents in picomoles added to 1×10^5 mAi9 cells in 500 μL of culture media in a 24-well format. (E) Top: Flow cytometry analysis of the percentage of tdTomato-positive mAi9 cells on day 4 following transfection with 7.5 pmol of Cas9/lox gRNA or with 7.5 pmol of Cas9SpC/lox gRNA to 5×10^4 mAi9 cells in 500 μL of culture media in a 24-well format. Cells a receiving mock treatment with phosphate-buffered saline were used to set the gate for detection of tdTomato-positive cells. Bottom: Scatter plot with a bar graph showing flow cytometry analysis of the percentage of tdTomato-positive cells on day 4 following transfection with Cas9/lox gRNA or with Cas9SpC/lox gRNA to mAi9 cells seeded at varying seeding cell densities in a 24-well format. Two replicate experiments were performed for parts C–E. Data are represented as mean ± standard deviation from six wells of two replicate experiments for parts C and D and as three wells of one representative experiment for part E.

protein and nucleic acid biologics, requires a delivery reagent to facilitate its intracellular uptake.[7,15,16] To date, gene editor RNPs have been delivered mainly using nonviral methods.[17−22] As an alternative, we hypothesized that gene therapy viral vectors for DNA delivery could be repurposed as a powerful carrier platform for intracellular delivery of RNPs. In this regard, adenovirus, in particular, possesses a number of salient features relevant to its employ as a robust RNP carrier. Adenoviral vectors have been engineered to efficiently infect a broad range of tissues with tissue specificity through the genetic capsid incorporation of targeting peptides or the use of targeting adapters.[23,24] Importantly, adenovirus has naturally evolved an infection pathway that can efficiently deliver viral DNA as well as its major capsid proteins into the cytoplasm of host cells.[25] This process involves the receptor-mediated endocytosis of whole virion particles by the host cell membrane followed by release of viral proteins and DNA to the cytoplasm through lysosomal mechanisms.[25−28] In this regard, our group demonstrated the adenoviral delivery of exogenous nucleic acids using a viral capsid conjugate system,

https://doi.org/10.1021/acsnano.2c00909
ACS Nano 2022, 16, 10443−10455

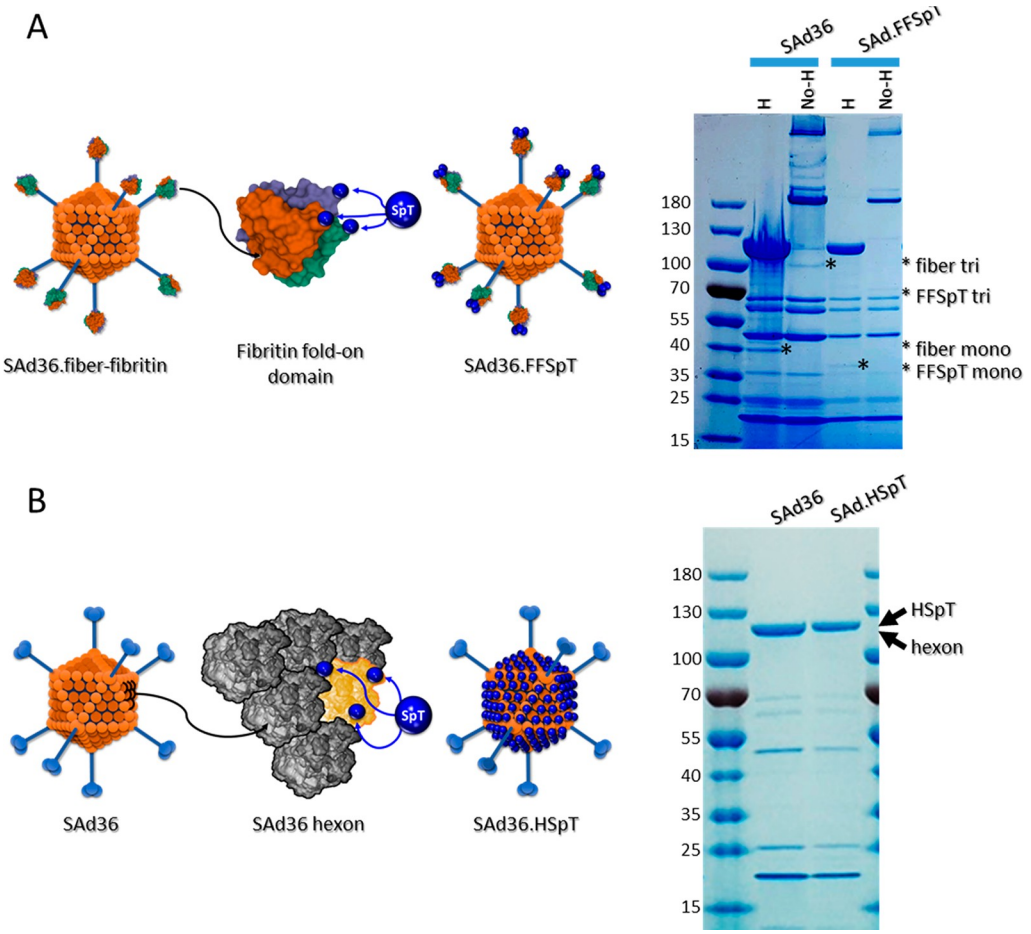

Figure 2. Generation of SAd36 vectors with SpT incorporated into the fiber and hexon. (A) Schema illustrating the SAd36 vector with the fiber knob domain replaced by the bacteriophage T4 fibritin fold-on domain which allows the outward display of SpT on the virus surface. The fiber-T4 fibritin-SpT (FFSpT) trimer is proportionally enlarged compared with the body of the virion for a clear presentation of the location of SpT. 2.5 × 10^{10} viral particles of SAd36 and SAd36.FFSpT were denatured in SDS sample buffer with or without boiling (H or No-H) for 8 min. Proteins were resolved by 4−15% gradient SDS-PAGE followed by Coomassie blue staining. The presence of FFSpT trimer (FFSpT tri) in the SAd36.FFSpT virus was detected in the sample treated without heating. (B) Schema illustrating the SAd36 vector with hexon hypervariable region 5 replaced by SpT. SAd36 and SAd36.HSpT viral particles were analyzed by SDS-PAGE and Coomassie blue staining with heating as described in part A.

where the adenovirus-bound nucleic acids were efficiently cointernalized and entered the cells along with other viral components, leading to therapeutic gene expression in target cells.[29,30] On this basis, we hypothesized that a preassembled Cas RNP complex conjugated on the surface of adenovirus would also be intracellularly delivered through the same mechanism.

Here we performed a proof-of-mechanism study and demonstrated highly efficient gene editing in cells infected with adenovirus carrying Cas9/gRNA on its capsid proteins. For this, we developed a recombinant protein−virus cross-linking strategy by employing a SpyTag003/SpyCatcher003 conjugation system.[31] In this system, a nuclear localization signal-loaded Cas9 was fused with SpyCatcher003, and the Cas9SpyCatcher003 protein possessed CRISPR nuclease activity comparable to that of a marketed Cas9. We further achieved the genetic incorporation of SpyTag003 to a simian adenovirus capsid fiber or hexon. Both SpyTag003 viruses potentiated efficient conjugation of Cas9SpyCatcher003 in a rapid, spontaneous, and titratable fashion. Cas9SpyCatcher003-conjugated viruses in the presence of a reporter gRNA delivered gene-editing capacity to cells in a dose-dependent fashion. The efficiency attained by the viral delivery approach was comparable to that of a commercial CRISPR/Cas transfection reagent.

RESULTS/DISCUSSION

Recombinant Cas9SpC Retained CRISPR Nuclease Activity. We sought to conjugate recombinant *Streptococcus pyogenes* Cas9 (SpCas9) to adenovirus and explore the viral infection pathway as a "piggyback" route to deliver CRISPR genome editing to target cells. We chose a third-generation SpyTag003/SpyCatcher003 system[31] to develop the protein−virus cross-linking approach. As expected, the covalent ligation chemistry between SpyCatcher003 (SpC hereafter) and SpyTag003 (SpT hereafter) in phosphate-buffered saline at 37 °C was spontaneous, occurred in a titratable fashion, and reached completion within 1−2 h (data not shown and Supporting Information Figure 1A and B). We next designed and produced SpCas9 incorporated with three nuclear localization signals (3xNLS_SpCas9)[32] in fusion with SpC_6xHis linked by a flexible peptide between the two moieties. The resultant 3xNLS_SpCas9_linker_SpC_6xHis (Cas9SpC hereafter) was about 20 kDa larger than the NLS-

https://doi.org/10.1021/acsnano.2c00909
ACS Nano 2022, 16, 10443−10455

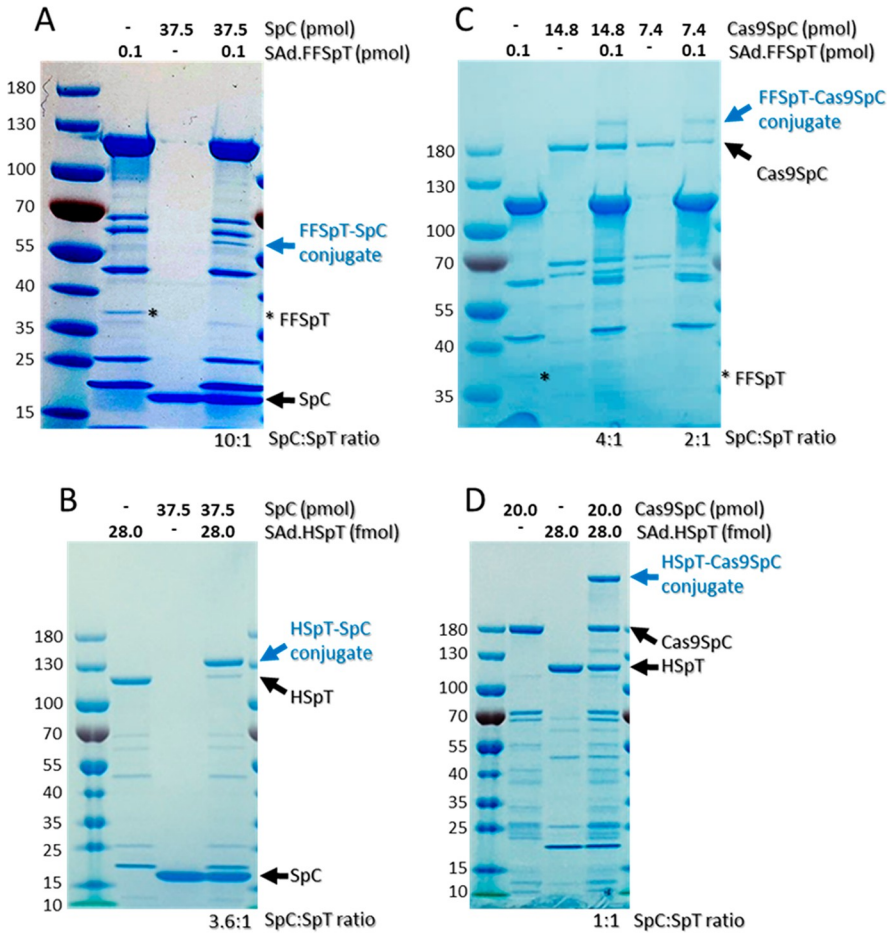

Figure 3. Covalent attachment of SpC and Cas9SpC to the SpT viruses. SAd36.FFSpT (A) or SAd36.HSpT (B) was incubated with SpC at the designated amounts at 37 °C for 2 h followed by boiling in SDS sample buffer and SDS-PAGE analysis with Coomassie staining. SAd36.FFSpT (C) or SAd36.HSpT (D) was incubated with Cas9SpC at the designated amounts at 37 °C for 2 h followed by boiling in SDS sample buffer and SDS-PAGE analysis with Coomassie staining. The molar ratio of SpC or Cas9SpC versus virus-incorporated SpT in the protein−virus conjugation reaction is provided under each lane.

incorporated TrueCut SpCas9 v2 (ThermoFisher Scientific; Figure 1A, left panel). Immunoblot analysis with SpCas9- and 6xHis-specific antibodies confirmed the identity of the produced protein (Figure 1A, middle and right panels). This protein, like SpC, showed complete accessibility for conjugation by SpT supplied in an excess amount, further confirming its identity as Cas9SpC (Supporting Information Figure 1C).

To test the CRISPR nuclease activity of Cas9SpC, we employed an NIH somatic cell genome editing (SCGE) program-established modified Ai9 (*Rosa26: Ai9-SauSpyCas9-tdTomato* or mAi9) reporter system available in both mice and cell line (MGI reference ID: J:302103; Figure 1B). In this system, a single guide RNA (lox gRNA) recognizing two sites flanking a transcriptional STOP cassette in the *Rosa26-tdTomato* locus directs Cas9-mediated dual cleavage and deletion of this cassette. The resultant dual-edited locus subsequently activates expression of downstream *tdTomato* gene, and as such, the red fluorescent protein signals serve as a surrogate marker for cells possessing the dual-edited allele. The TrueCut Cas9 v2 (Cas9 hereafter)/lox gRNA was included as a CRISPR nuclease activity reference control, and delivery of the editors to mAi9 mouse embryonic fibroblasts was achieved using lipofectamine CRISPRMAX reagent. Robust CRISPR gene editing was detected in cells receiving Cas9/lox gRNA as well as in cells receiving Cas9SpC/lox gRNA (Supporting Information Figure 2; Figure 1C−E). The dose response by varying the amount of both Cas9SpC (Supporting Information Figure 2A; Figure 1C) and lox gRNA (Supporting Information Figure 2B; Figure 1D) and by changing the seeding cell density (Figure 1E) defined an optimized dose regimen/cell density that produced 33.3% ± 9.3% (mean ± SD hereafter) dual-edited cells by flow cytometry analysis. The equivalent molar dose of Cas9/gRNA yielded 38.0% ± 1.0% dual-edited cells, suggesting that Cas9SpC possessed about 88% of Cas9 nuclease activity.

Genetic Incorporation of SpT into Simian Adenovirus 36 Capsid Proteins for Functional Anchoring. We chose simian (chimpanzee) adenovirus species E serotype 36 (SAd36)[33] to engineer SpT-incorporated virus. SAd36 showed low prevalence of pre-existing neutralizing antibodies in human populations[34] and has recently emerged as a vaccine platform in preclinical studies and clinical trials with a favorable safety profile.[35−37] Importantly, SAd36 exhibited low native tropism in mice when systemically administered but achieved efficient vector targeting via genetic modification of capsid proteins, making it a promising vector for clinical targeted gene therapy applications (unpublished data; manuscript in preparation). To this end, we have successfully derived SAd36 with SpT incorporated into two capsid proteins, fiber and hexon. In the

https://doi.org/10.1021/acsnano.2c00909
ACS Nano 2022, 16, 10443−10455

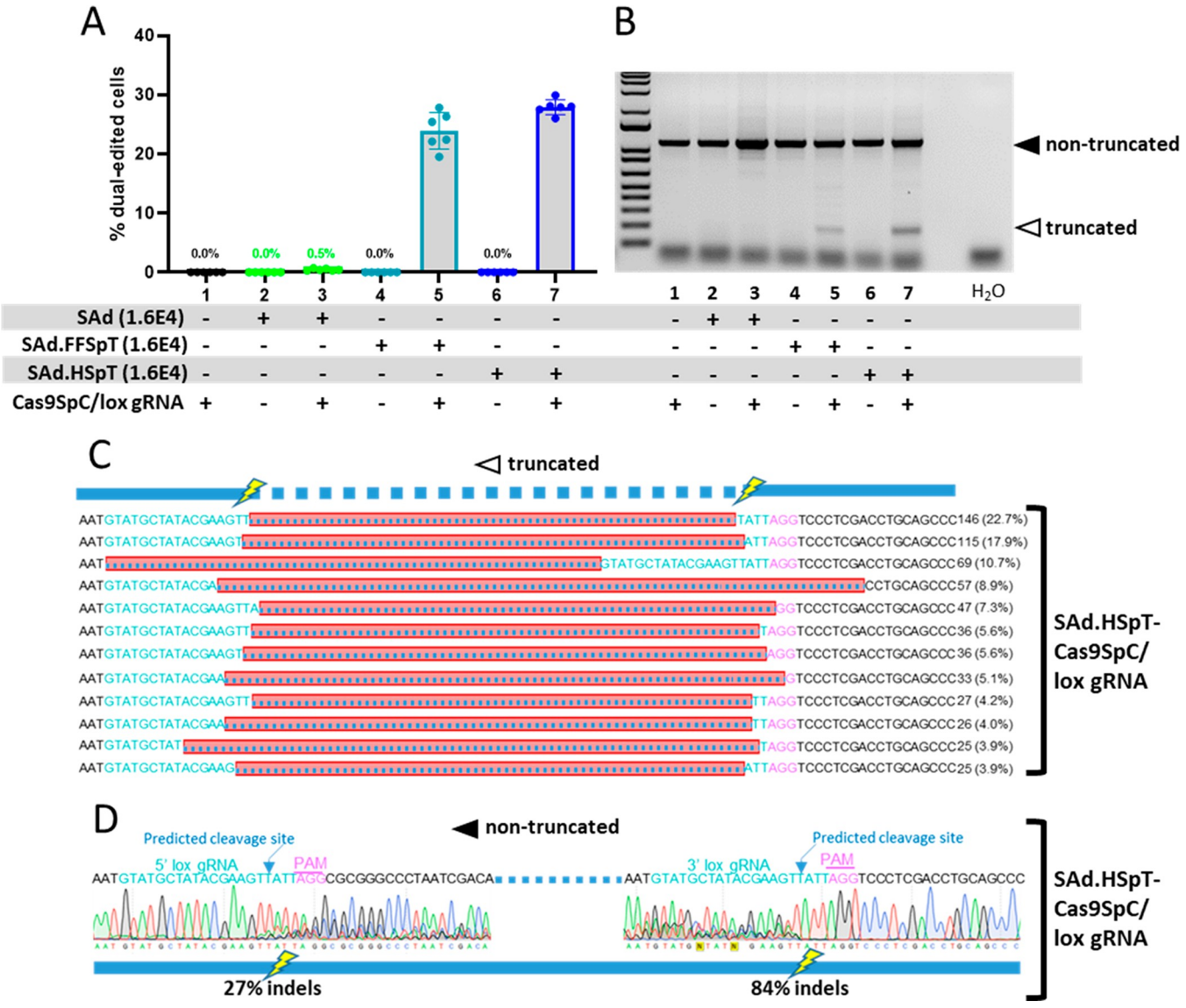

Figure 4. Efficient gene editing in cells infected with SpT SAd36 vectors carrying Cas9SpC/gRNA on capsid proteins. (A) Scatter plot with a bar graph showing the percentage of tdTomato-positive cells by fluorescence microscopy analysis of mAi9 cells on day 4 following virus infection. For this, 2×10^5 modified Ai9 cells in 500 μL of culture media in a 24-well format were incubated with SAd36, SAd36.FFSpT, and SAd36.HSpT at a 1.6×10^4 viral particles per cell ratio without or with a 2-h preincubation of 7.5 pmol of Cas9SpC/lox gRNA. Two replicate experiments were performed, and data are represented as mean ± standard deviation from six wells of the two experiments. (B) Genotyping PCR analysis of the *ROSA26-tdTomato* locus using DNA samples derived from cells in one of the experiments shown in part A. The locations of the PCR primers (F and R) are illustrated in Figure 1B. Solid arrowhead, predicted nontruncated PCR band; hollow arrowhead, truncated PCR fragments. (C) Next-generation sequencing analysis of the truncated Rosa26-tdTomato PCR fragment amplified with genomic DNA derived from cells infected with SAd36.HSpT-Cas9SpC/lox gRNA, indicated by the hollow arrowhead in part B. The location of various deletion species (boxed dash lines) and the corresponding number of times of detection are provided. The numbers in parentheses report the frequency of detection of a particular deletion species from all sequencing reads. (D) ICE analysis of the nontruncated Rosa26-tdTomato PCR fragment amplified using genomic DNA derived from cells infected with SAd36.HSpT-Cas9SpC/lox gRNA. DNA was isolated 4 days post virus infection. The overall indel frequencies at both upstream and downstream lox gRNA sites are provided, and a detailed report of the assay is provide in Supporting Information Figure 7C.

former, the fiber knob domain with an inward C-terminus was replaced by a bacteriophage T4 fibritin fold-on domain with an outward C-terminus to display SpT, yielding the SAd36.fiber-T4 fibritin-SpT (SAd36.FFSpT) vector (Supporting Information Figure 3A). Importantly, the T4 fibritin domain also provided the fiber trimerization function of the knob domain, which was required for successful virion assembly.[38] In the hexon, an outward, 9-residue hypervariable region 5 loop was identified via phylogenetic analysis of human and simian viral proteins and replaced with SpT flanked by two 15-residue flexible linkers, producing the SAd36.hexon-SpT (SAd36.HSpT) vector (Supporting Information Figure 3B). The two SpT vectors differed significantly in the abundance of SpT displayed on the virion surface with 36 FFSpT monomers and 720 HSpT monomers per virion, respectively (Figure 2A and B, left panels). Viruses were successfully rescued from the two SpT viral genomes, and both viruses grew robustly during upscaling and yielded high-titer preparations. Viral protein

https://doi.org/10.1021/acsnano.2c00909
ACS Nano 2022, 16, 10443−10455

composition analysis revealed the presence of protein bands with predicted molecular weights of the modified fiber and modified hexon in respective viral preparations (Figure 2A and B, right panels).

Efficient Covalent Attachment of Cas9SpC to Virus Capsid via SpT Anchor. The conjugation chemistry between SpT and SpC is highly specific.[31] Consistent with this notion, there was a lack of detectable nonspecific covalent cross-linking between Cas9SpC and wild-type SAd36 viral proteins following a 2-h incubation (Supporting Information Figure 4). We intended to incorporate SpT into sites on the fiber and hexon for its optimal accessibility to SpC and, therefore, tested the reactivity of SpC to SAd36.FFSpT and SAd36.HSpT using the same assay. An excess amount of SpC versus viral SpT abundance efficiently titrated FFSpT and HSpT to SpC-conjugate forms (Figure 3A, FFSpT-SpC conjugate; Figure 3B, HSpT-SpC conjugate), thus validating our vector engineering design. Compared with the small SpC protein of 15 kDa, the molecular weight of Cas9SpC is 180 kDa. In this regard, the bulky Cas9SpC retained the capacity of conjugation with all 36 FFSpT sites on the virion (Figure 3C). The Cas9SpC also efficiently converted about half of the 720 HSpT sites to the Cas9SpC-conjugate form (Figure 3D), implying that steric hindrance between free and virus-conjugated Cas9SpC molecules prevented the conjugation of the rest of the viral HSpT sites. Transmission electron microscopy analysis revealed an indistinguishable virion morphology among SAd36, SAd36.FFSpT, and SAd36.HSpT and confirmed that conjugation of Cas9SpC on SAd36.FFSpT and SAd36.HSpT surfaces had a minimal impact on the virion morphology (Supporting Information Figure 5).

In aggregate, we pioneered a modular synthetic approach to efficiently derive adenoviral vectors carrying a large and complex functionality on the virus surface. Specifically, we successfully introduced SpT onto two different surface sites of SAd36 and subsequently achieved cross-linking of a Cas9 moiety (160 kDa) fused with SpC (15 kDa) to the engineered viruses. Noticeably, our approach overcomes some of the limitations of current adenoviral engineering technologies. First, while the genetic capsid modification approach has made feasible the incorporation of peptide and, with some success, small proteins such as single-domain antibodies (~15 kDa) and even single-chain variable fragments (~27 Da) into capsid proteins,[24] the rescuability of the modified viral genomes varies tremendously and needs to be experimentally determined. On the other hand, there has been no report yet on the use of the virus adapter strategy to add functionalities to rare human or nonhuman adenoviral vectors, largely due to the unavailability of viral serotype-specific capsid binders. In these regards, we demonstrated that SpT-incorporated viral vectors as well as the SpC fusion protein could be produced and functionally validated before assembly, and an "off-the-shelf" mixing of the two components under physiological conditions led to a spontaneous titration reaction producing desired adenoviral vectors displaying the macromolecules on the surface. On this basis, we anticipate that adenoviruses employing this protein–virus conjugation system will readily provide a versatile plug-and-play macromolecule display platform for broader applications including development of targeted delivery systems, adenoviral vectors with shielding against neutralizing antibodies, and protein-based vaccines.

Efficient Gene Editing in Cells Infected with SpT SAd36 Vectors Carrying Cas9SpC/gRNA on the Virion Surface. We defined the infectivity of SAd36, SAd36.FFSpT, and SAd36.HSpT to mAi9 cells using a fixed 1.6×10^4 viral particle to cell (VP/C) ratio based on expression of viral green fluorescent protein (GFP) reporter gene driven by the major immediate-early promoter/enhancer of human cytomegalovirus (CMV). Compared with 25% GFP^+ cells by the SAd36 on day 1 post infection, FFSpT virus produced slightly reduced 17% GFP^+ cells, and HSpT virus yielded a noticeable increase in GFP^+ cells to 33% (Supporting Information Figure 6A, columns 2, 4, 6, GFP). These results indicated that the fiber knob domain played a minor role in shaping the SAd36 infectivity of mAi9 cells, and the molecular basis for the increased infectivity of the hexon-modified virus remains to be defined. All three viruses were also incubated with Cas9SpC for 2 h followed by addition of equal moles of lox gRNA, and the resultant reaction mixtures retained the infection levels of all three viruses without Cas9SpC/lox gRNA (Supporting Information Figure 6A, 3 versus 2, 5 versus 4, and 7 versus 6, GFP). Importantly, these results suggested that the negatively charged Cas9SpC/lox gRNA complex conjugated on the virion surface affected little with respect to its infection of mAi9 cells.

We next determined whether the viral "piggyback" mechanism had the capacity of inducing genome editing in infected cells. We first ruled out the possibility that Cas9SpC/lox gRNA, alone or when added to cell culture medium, could produce any detectable gene editing at the *Rosa26-tdTomato* locus in mAi9 cells (Supporting Information Figure 6A, column 1-tdT; Figure 4A, bar 1). We further showed that infection of SAd36, SAd36.FFSpT, or SAd36.HSpT did not yield any detectable gene-editing events (Supporting Information Figure 6A, columns 2, 4, and 6, tdT; Figure 4A, bars 2, 4, and 6). In contrast, premixing of SAd36.FFSpT or SAd36.HSpT with Cas9SpC/lox gRNA produced efficient gene editing at the *Rosa26-tdTomato* locus, leading to 23.9% ± 3.1% and 27.9% ± 1.3% dual-edited cells, respectively (Supporting Information Figure 6A, columns 5 and 7, tdT; Figure 4A, bars 5 and 7). Intriguingly, a very low yet highly reproducible 0.5% ± 0.1% dual-gene-editing level was detected in cells treated with the SAd36 and Cas9SpC/gRNA mixture (Supporting Information Figure 6A, column 3-tdT; Figure 4A, bar 3), implying that, while mAi9 cells did not take up naked Cas9SpC/lox gRNA, uptake of SAd36 by the cells triggered a low-level codelivery of the RNP complex by an undefined mechanism. Next, a PCR genotyping analysis of the *Rosa26-tdTomato* locus (Figure 1B, primers F and R) with genomic DNA derived from cells analyzed in Figure 4A amplified a predicted nontruncated fragment in all samples (Figure 4B, all lanes, solid arrowhead). In addition, the assay detected truncated fragments in the two samples from cells infected with SAd36.FFSpT-Cas9SpC/lox gRNA and with SAd36.HSpT-Cas9SpC/lox gRNA (Figure 4B, lanes 5 and 7, hollow arrowhead). Next-generation DNA sequencing analysis of the truncated bands from the two groups confirmed Cas9-mediated double-stranded DNA cleavage at both lox gRNA sites resulting in deletion of the STOP cassette (Supporting Information Figure 7A, SAd.FFSpT-Cas9SpC/lox gRNA; Figure 4C, SAd.HSpT-Cas9SpC/lox gRNA). Furthermore, we performed Sanger sequencing of the nontruncated band followed by inference of CRISPR edits (ICE) analysis to measure the level of Cas9-induced DNA double-strand breaks repaired by nonhomologous end joining (NHEJ) (https://ice.synthego.com/#/).[39] Cells infected with SAd36.FFSpT-Cas9SpC/lox gRNA exhibited 17% and 27% small insertion/

https://doi.org/10.1021/acsnano.2c00909
ACS Nano 2022, 16, 10443–10455

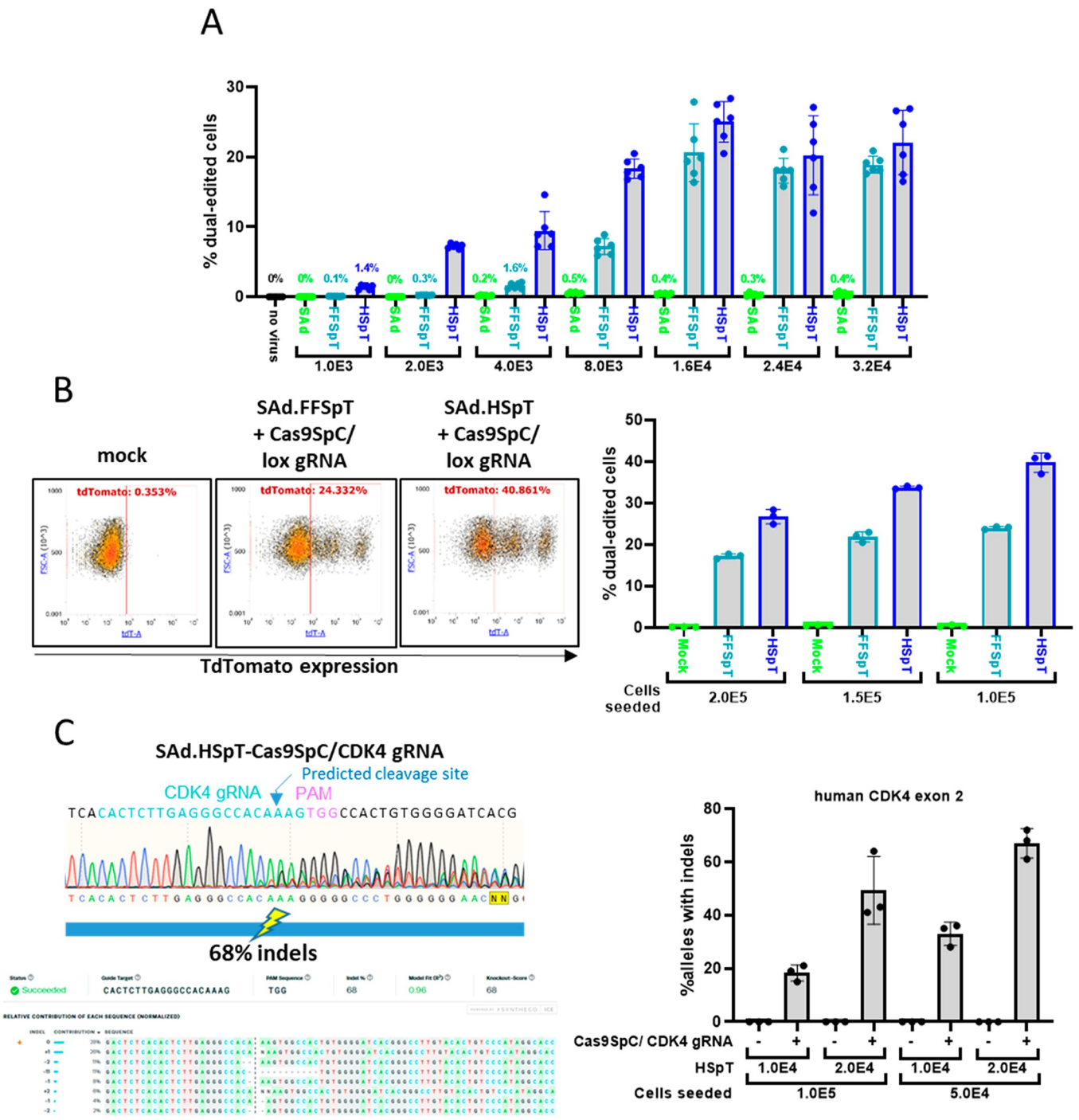

Figure 5. Viral dose and cell confluence level-dependent gene editing delivered by SpT SAd36 vectors carrying Cas9SpC/gRNA. (A) Scatter plot with a bar graph showing the percentage of tdTomato-positive cells by fluorescence microscopy analysis of mAi9 cells on day 4 following virus infection. Specifically, 2 × 10^5 modified Ai9 cells were incubated with varying amounts of SAd36, SAd36.FFSpT, and SAd36.HSpT in the presence of 7.5 pmol of Cas9SpC/lox gRNA. The viral particle versus cell ratios are provided at the bottom of the plot. (B) Left: Flow cytometry analysis of the percentage of tdTomato-positive cells on day 4 following infection of 1.0 × 10^5 mAi9 cells with SAd36.FFSpT-Cas9SpC/lox gRNA or SAd36.HSpT-Cas9SpC/lox gRNA at a 1.6 × 10^4 VP/C ratio. Cells receiving mock treatment with phosphate-buffered saline were used to set the gate for detection of tdTomato-positive cells. Right: Scatter plot with a bar graph showing flow cytometry analysis of the percentage of tdTomato-positive cells on day 4 following infection with SAd36.FFSpT-Cas9SpC/lox gRNA or SAd36.HSpT-Cas9SpC/lox gRNA at a 1.6 × 10^4 VP/C ratio to cells with three different seeding densities: 2.0 × 10^5, 1.5 × 10^5, and 1.0 × 10^5 per well in a 24-well format. (C) Left panel: ICE analysis of the *CDK4* locus PCR fragment amplified using genomic DNA derived from A549 cells (5.0 × 10^4/well) infected with SAd36.HSpT-Cas9SpC/CDK4 gRNA at a 2.0 × 10^4 VP/C ratio. Genomic DNA was purified on day 2 post virus infection. Right panel: Scatter plot with a bar graph showing ICE analysis of the percentage of CDK4 alleles harboring Cas9SpC-mediated indels on day 2 following infection with SAd36.HSpT-Cas9SpC/CDK4 gRNA at a 1.0 × 10^4 or 2.0 × 10^4 VP/C ratio to cells with two different seeding densities of 1.0 × 10^5 or 0.5 × 10^4 per well in a 24-well format. Two replicate experiments were performed for parts A–C. Data are represented as mean ± standard deviation from six wells of two replicate experiments for part A and three wells of one representative experiment for parts B and C.

https://doi.org/10.1021/acsnano.2c00909
ACS Nano 2022, 16, 10443–10455

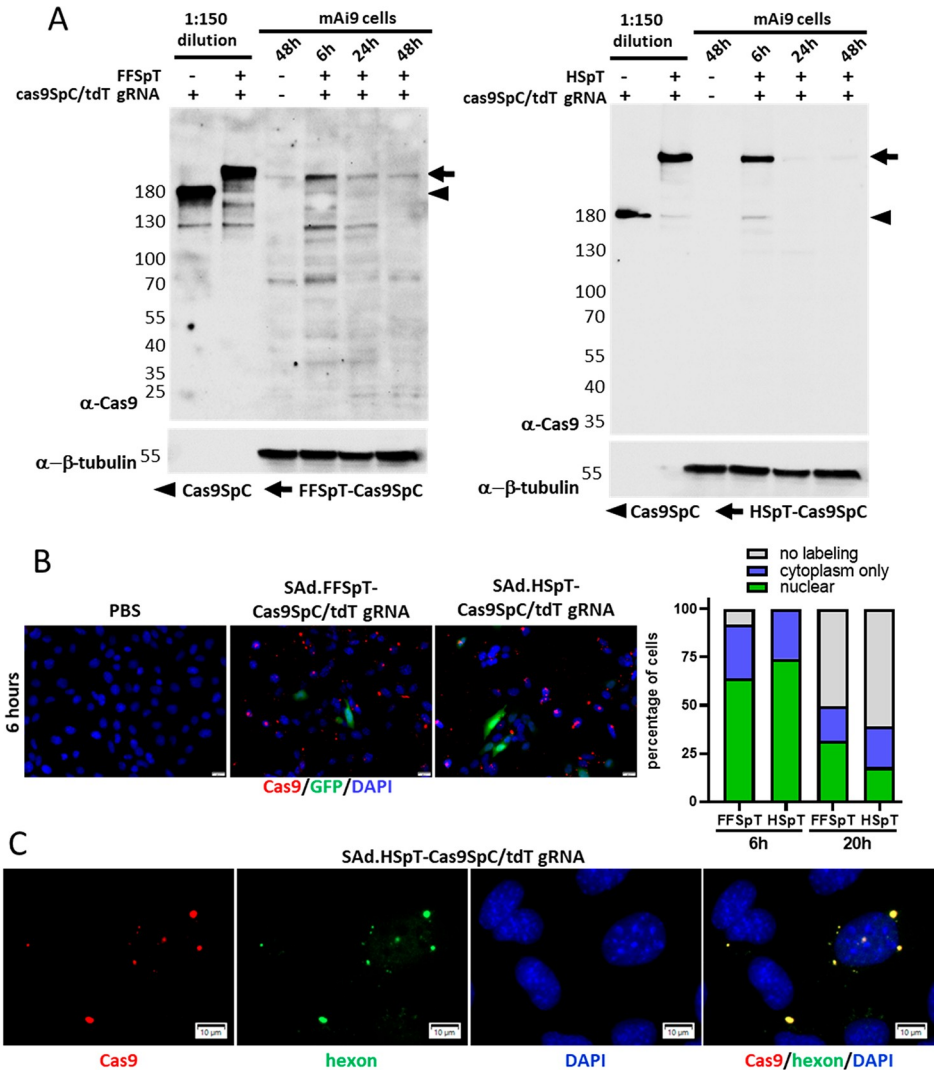

Figure 6. Intracellular delivery of conjugated "piggyback" Cas9SpC by SpT SAd36 viruses. (A) Left panel: Immunoblot analysis of free Cas9SpC, Cas9SpC conjugated on SAd36.FFSpT, and the fate of the Cas9SpC−FFSpT conjugate in mAi9 cells following infection with SAd36.FFSpT-Cas9SpC/tdT gRNA at a 1.6 × 10^4 VP/C ratio. Right panel: Immunoblot analysis of free Cas9SpC, Cas9SpC conjugated on SAd36.HSpT, and the fate of Cas9SpC-HSpT in mAi9 cells following infection with SAd36.HSpT-Cas9SpC/tdT gRNA at a 1.6 × 10^4 VP/C ratio. The tdT gRNA sequence is 5′-ggccacgagttcgagatcga-3′ followed by a PAM sequence of 5′-ggg-3′. The tdT gRNA recognizes two sites in *tdTomato* gene as this gene itself is a genetic fusion of two copies of a *dTomato* gene. (B) Immunofluorescence microscopy analysis of subcellular localization of the Cas9 moiety in virus-infected mAi9 cells. Strikingly, robust GFP fluorescence signals without antibody staining were readily detectable in a small number of cells by 6 h post virus infection. Magnification, ×40. Red, Cas9 moiety; green, GFP; blue, DAPI. Right panel: DAPI staining revealed the nucleus of each cell, and subcellular localization of the Cas9 moiety versus the nucleus location in all assayed cells was scored. The bar graph illustrates the percentage of cells showing nuclear Cas9 detection, cytoplasm-only Cas9 staining, or no cellular Cas9 detection in individual virus/time groups. (C) Co-immunofluorescence staining of the Cas9 moiety and SAd36 hexon in cells at 6 h post virus infection detected colocalization of the two protein moieties. Cas9 and hexon were revealed in the Texas Red and Cy5 (far-red)-channels, respectively, and the hexon staining was pseudocolored in green. Magnifications, ×100. Red, Cas9; green, hexon; blue, DAPI.

deletion (indel)-type Cas9 editing at the upstream and downstream lox RNA sites from all nontruncated alleles, respectively (Supporting Information Figure 7B), while cells infected with SAd36.HSpT-Cas9SpC/lox gRNA showed 27% and 84% editing at the two sites (Figure 4D; Supporting Information Figure 7C). Taken together, the combined results from Figure 4C and D suggested that cells infected with SAd36.FFSpT-Cas9SpC/lox gRNA exhibited 37% editing of all alleles at upstream and 45% at downstream lox RNA recognition sites, and cells infected with SAd36.HSpT-Cas9SpC/lox gRNA exhibited 47% editing of all alleles at upstream and 89% at downstream lox RNA recognition sites.

Next, the virus dose response by varying the VP/C ratio to cells seeded at 2.0 × 10^5 per well in a 24-well format revealed superior gene-editing activity by SAd36.HSpT-Cas9SpC/lox gRNA over SAd36.FFSpT-Cas9SpC/lox gRNA at lower VP/C ratios (Supporting Information Figure 6B; Figure 5A, FFSpT and HSpT/1.0−8.0 × 10^3 VP/C). Thus, HSpT virus at a VP/C ratio of 8.0 × 10^3 attained an 18.4% ± 1.4% dual-editing level versus 7.2% ± 1.4% by the FFSpT equivalent. Both FFSpT and HpT viruses, however, reached a plateau of gene-editing efficiency at VP/C ratios higher than 1.6 × 10^4 (Supporting Information Figure 6B; Figure 5A, FFSpT and HSpT/2.4 × 10^4 and 3.6 × 10^4 VP/C), implying that, at high

https://doi.org/10.1021/acsnano.2c00909
ACS Nano 2022, 16, 10443−10455

VP/C ratios, nuclear entry of FFSpT-Cas9SpC/gRNA was almost as effective as HSpT-Cas9SpC/gRNA, although the FFSpT virus contained about 10 times less Cas9SpC than the HSpT virus. We further showed that the capacity of the viral "piggyback" genome editing was also sensitive to the cell confluence level with cells seeded at 1.0×10^5 per well in a 24-well format supporting the most efficient gene editing by both SpT SAd36 vectors carrying Cas9SpC/lox gRNA. In this regard, FFSpT and HSpT viruses at 1.6×10^4 VP/C ratio produced 24.1% ± 0.4% and 39.7% ± 2.3% dual-editing, respectively, on day 4 following virus infection (Figure 5B, right panel, cells seeded: 1.0×10^5 per well). We further investigated the effects of viral dose and seeding cell density on gene-editing efficiency by SAd36.HSpT-Cas9SpC at the *CDK4* locus in human lung adenocarcinoma A549 cells. A superior editing efficiency of 67.0% ± 5.6% (indels) of all *CDK4* alleles was attained in cells seeded at 5.0×10^4 per well in a 24-well format and infected with SAd36.HSpT-Cas9SpC/CDK4 gRNA at a 2.0×10^4 VP/C ratio (Figure 5C). Taken together, these data fully validated the feasibility of achieving efficient gene editing by the adenoviral "piggyback" delivery route of the editor machinery in both murine and human cells.

To gain a mechanistic understanding of the adenoviral "piggyback" transport of the Cas9/gRNA complex, we next studied the fate of Cas9SpC conjugated on SpT viruses following infection of mAi9 cells. A tdTomato-specific gRNA instead of the lox gRNA was used in the following assays to allow the proper intranuclear localization of Cas9SpC/gRNA complex yet avoid the activation of *tdTomato* gene expression. Immunoblot analysis with the SpCas9-specific antibody revealed abundant FFSpT-Cas9SpC (219.1 kDa) and HSpT-Cas9SpC (288.7 kDa) conjugates in cells at 6 h post infection with SAd36.FFSpT-Cas9SpC/tdT gRNA or SAd36.HSpT-Cas9SpC/tdT gRNA (Figure 6A and B, 6 h, arrows). The cellular levels of capsid−Cas9SpC conjugates reduced markedly by 24 h post infection but remained slightly above the detection threshold by 48 h post infection (Figure 6A and B, 24 h and 48 h, arrows). Immunofluorescence (IF) microscopy analysis revealed Cas9 staining in a majority of cells at 6 h post virus infection with greater than half of all assayed cells possessing nuclear Cas9 signals and a small portion of cells containing cytoplasm-only Cas9 presence (Figure 6B). In addition, we validated the reactivity of a goat polyclonal antibody against human adenovirus 5 hexon to the SAd36 equivalent by IF studies (data not shown). Consistent with the immunoblot results, costaining of cells at 6 h post virus infection with Cas9 and SAd36 hexon antibodies showed a striking colocalization of the two protein moieties within infected cells (Figure 6C). Together, these data raised the possibility that nuclear FFSpT-Cas9SpC/gRNA and HSpT-Cas9SpC/gRNA may retain the CRISPR nuclease activity that was responsible for gene editing in infected cells. Consistent with this notion, we carried out an *in vitro* DNA cleavage assay on a PCR-generated *Rosa26-tdTomato* fragment using Cas9SpC/gRNA conjugated on both SpT viruses as shown in Figure 6A (lane 2 of both immunoblot panels). The free Cas9SpC and two-capsid-linked Cas9SpC with the lox gRNA as well as with a second mAi9 gRNA (gRNA2) robustly cleaved the fragment to completion when compared with the free Cas9 (Supporting Information Figure 8), suggesting that Cas9 in fusion with SpC (i.e. Cas9SpC) or Cas9SpC conjugated on SpT virus capsids did not affect nuclease activity when compared with free Cas9.

A salient finding of the present study was the utility of the adenoviral capsid conjugate approach to deliver an intracellularly acting macromolecule, the cas9/gRNA RNP complex. Till now, a number of attempts have been made to achieve intracellular delivery of protein and RNP biologics to human cells using nonviral carriers such as cationic liposomes,[17] cell-penetrating peptide incorporation,[18] anionic polymers,[19] and nanocapsule polymers.[21] A major limiting factor is presently the lack of a defined *in vivo* targeted delivery mechanism to arm these systems, which is the focus of current research. Unlike the emerging nonviral approaches, adenovirus is one of the commonly utilized gene therapy platforms due to the availability of a collection of vectors with diverse tissue tropism across a variety of disorders.[23,24,40] As detailed in the introduction section, additional advantages have made the adenoviral vector an ideal exogenous protein and RNP delivery platform. Interestingly, adenovirus possesses a very efficient nuclear entry mechanism for viral DNA as well as capsid proteins.[26] Our data are consistent with the notion that the NLS-loaded gene editor conjugated on the adenoviral fiber or hexon can efficiently gain access to the host cell nuclear compartment and function normally as a gRNA sequence-mediated DNA endonuclease on chromatin DNA, revealing compatibility of the conjugated capsid proteins to subnuclear localization of NLS-Cas9 nuclease. However, to generalize the utility of the viral delivery platform for other cellular biologics, it is potentially crucial to provide a releasable function to the protein cargo moiety from the capsid conjugate within the cytoplasm or inside the nucleus. In this regard, the use of an integral viral protease-cleavable linker[22] and intracellular biodegradable cross-linking scheme[19] has been reported to attain the intracellular release of a protein cargo from its conjugate. Notably, as an integral core protein within mature adenoviral particles, adenovirus L3 protease (AVP) activity is believed to play a critical role in facilitating a series of viral capsid uncoating events in the endosome and cytoplasm.[25,41] As such, an attractive hypothesis warranting further research is the introduction of an AVP preferential cleavage site at the linker between the protein cargo and SpC to facilitate the release of protein cargo in the cytoplasm.

An intriguing aspect of the adenoviral Cas9/gRNA RNP delivery is related to the question of whether a similar efficient RNP delivery can be achieved with viral particles composed of empty capsids without viral DNA in a potential adenoviral-like particle platform. In this regard, adenovirus assembly follows a sequential pathway in which the formation of empty capsids containing the major and minor capsid proteins and some core components such as AVP protease precedes genome packaging into the empty capsids to form mature full virions.[42,43] The DNA-free empty capsids with a lower density are readily detectable and separable from the heavier full virions during a routine virus purification procedure. The hypothesis that the SpT-incorporated empty capsids may possess the full capacity of gene editor cargo conjugation and delivery to the reporter cells is currently under investigation.[42]

CONCLUSION

We described the development of a plug-and-play adenoviral platform that can piggyback transport Cas9/gRNA complex on viral capsid surface into the nucleus of target cells, leading to robust genome editing. This viral intracellular delivery system works via a spontaneous titration reaction between the off-the-shelf engineered virus and a prevalidated Cas9/gRNA complex

https://doi.org/10.1021/acsnano.2c00909
ACS Nano 2022, 16, 10443−10455

exploiting SpyTag003/Spycatcher003 coupling chemistry under physiological conditions. The resultant Cas9/gRNA-conjugated virus was employed directly to achieve robust gene editing in target cells. As such, the repurposed utility of a clinically relevant adenoviral vector establishes the technical basis for a range of interventional possibilities.

MATERIALS AND METHODS

Materials. TrueCut Cas9 V2 was purchased from ThermoFisher Scientific. SpyCatcher003 and SpyTag003-MBP proteins were acquired from Kerafast, Inc. Lox sgRNA targets the DNA sequence 5′-GTATGCTATACGAAGTTATT-3′. mAi9 sgRNA2 targets 5′-AAGTAAAACCTCTACAAATG-3′. The *tdTomato* gene knockout sgRNA recognizes 5′-GGCCACGAGTTCGAGATCGA-3′. Human CD4 exon 2 sgRNA recognizes 5′-CACTCTTGAGGGCCACAAAG-3′. The Cas9 sgRNAs were custom-synthesized using TrueGuide synthetic CRISPR gRNA technology with chemical modifications including 2′-*O*-methyl analogs and phosphorothioate linkages which increase editing efficiency and protect against nuclease degradation. Modified Ai9 (Ai9-SauSpyCas9 or mAi9) mouse embryonic fibroblasts were acquired from Jason Heaney of Baylor University.

Cas9SpC Cloning and Expression. The plasmid pET-21a_3xNLS_SpCas9_protein_expression was a gift from Scot Wolfe (Addgene plasmid # 114365; http://n2t.net/addgene:114365; RRID:Addgene_114365). The SpCas9 cassette is armed with three nuclear localization signals and contains at its 5′-end the T7 phage gene 10 leader sequence that enhances translation of foreign mRNAs in *E. coli*. A digestion of pET-21a_3xNLS_SpCas9 plasmid with XhoI and DraIII released a 6xHis tag-containing fragment. A 856 bp fragment with a TEV protease recognition site, SpyCatcher003, and 6xHis was synthesized and ligated via Gibson assembly to the XhoI/DraIII-digested pET-21a_3xNLS_SpCas9 backbone to yield the 3xNLS_SpCas9_SpyCatcher003_6xHis fusion cassette. The resultant plasmid was introduced into protein expression BL21(DE3) *E. coli* cells. Single colonies were used to inoculate 100 mL of starter LB containing 100 μg/mL carbenicillin and grown at 37 °C with shaking at 250 rpm until the OD_{600} of the culture reached 1.9. A. Fresh LB (0.5 L) was inoculated with the starter culture with initial OD_{600} at 0.01 and was grown at 37 °C with shaking at 250 rpm until the OD_{600} reached 0.5−0.8. Recombinant protein expression was induced with 0.42 mM isopropyl β-D-1-thiogalactopyranoside (IPTG) in medium, and the cultures were incubated overnight at 21 °C with shaking at 250 rpm. Cultures were centrifuged, and cell pellets were resuspended in lysis buffer (0.5 mM Tris, 0.3 M NaCl, 10 mM imidazole, 0.2% Triton, 1 mg/mL lysozyme, 20 units/mL DNase I, 1 mM PMSF, and one cOmplete mini EDTA-free protease inhibitor cocktail tablet per 10 mL) and incubated at 37 °C for 30 min. The cell lysates were clarified by centrifugation at 32,000 rcf at 4 °C for 30 min, the 6×His-tagged recombinant protein was purified using a HisPur Ni-NTA column with 20 mM imidazole washing buffer and 300 mM imidazole elution buffer, and eluted proteins were dialyzed in 10% glycerol in PBS with three buffer changes using 3.5 KDa molecular weight cutoff Slide-A-Lyzer Dialysis Cassettes. Protein concentration was measured using absorbance at 280 nM with extinction coefficient calculated by SnapGene software.

Construction of Recombinant SpT SAd36 Vectors. We employed pC36.000.cmv.PI.EGFP.BGH plasmid carrying the genome of chimpanzee adenovirus SAd36 from species/subgroup E, in which the early E1 region was replaced by a CMV promoter-hybrid intron-eGFP cassette. We further engineered E3 region-deleted pC36.000.cmv.PI.EGFP.BGH viral genome by removing a 4384 bp fragment from a BspEI site to the E3 14.7K stop codon, which includes seven genes: E3 CR1-α, E3 gp19K, E3 CR1-β, E3CR1-γ, E3 RID α, E3 RID β, and E3 14.7k.[35] To engineer SAd36 fiber modification, we created a pSAd36 fiber shuttle vector, in which a 4642 bp fragment from the SwaI site to the downstream ITR was cloned into an Amp-resistance plasmid backbone. The fiber knob region (sequences encoding codon 246 to the last codon 425) was replaced by the 285 bp bacteriophage T4 fibritin domain, 45 bp sequence encoding a flexible linker, and sequences encoding SpyTag003 to derive the pSAd36-FFSpT shuttle. The viral genome fragment within the pSad36FFSpT shuttle was released with two engineered restriction enzyme SacII and StuI sites and ligated back to the rest of the pSAd36 viral backbone scarlessly via Gibson assembly to derive pSAd36.FFSpT. We also created a pSAd36 hexon shuttle vector, in which a 4398 bp ClaI-SbfI fragment was cloned into the Amp-resistance plasmid backbone pre-engineered with adapter sequences containing ClaI-SbfI sites as well as flanking viral sequences. The hexon hypervariable region 5 (sequences encoding codon 257 to codon 301) was replaced by 48 bp SpyTag003 flanked by 45 bp at the 5′ end and 42 bp at 3′ sequences encoding flexible linkers to derive the pSAd36-HVR5-45AA-SpyTag shuttle. The viral DNA was released from the shuttle vector with MluI and *Hpa*I sites and reintroduced back to the rest of the viral genome cut with dual ClaI-SbfI via Gibson assembly to derive the pSAd36.HSpT viral genome. The constructed viral genomes were excised by restriction PacI digestion and then transfected into 293F28 cells for SAd36.FFSpT or into 293 cells for SAd36.HSpT. The in-house 293F28 system was derived from HEK293 cells engineered to express wild-type Ad5 fiber protein, which was able to trans-complement pSAd36.FFSpT for the lack of wild-type SAd36 fiber function in virus rescue and upscaling. SAd36.FFSpT was subject to a final propagation in unmodified HEK293 cells to obtain viral particles containing only the chimeric FF-targeting peptide. Hexon-modified virus was upscaled with HEK293 cells. Viruses were purified by CsCl gradient centrifugation and dialyzed against 10% glycerol in PBS, and viral particle titer will be quantified by measuring the absorbance of the dissociated virus at 260 nm using a conversion factor of 1.1×10^{12} viral particles (vp) per absorbance unit.

SDS-PAGE Coomassie Blue Staining and Immunoblot Analysis. Protein samples were mixed with 0.5 volume of 3× SDS sample buffer (187.5 mM Tris-HCl, pH 6.8, 6% SDS, 30% glycerol and 0.03% bromophenol blue, 0.125 M dithiothreitol) and heated at 97 °C or boiling for 8 min. Protein samples were also treated at room temperature for 8 min as a no-heating control. Treated protein samples were resolved by 4−15% gradient SDS-PAGE using a Criterion electrophoresis system (Bio-Rad), and gels were washed with water briefly and stained with GelCode blue stain reagent (FisherScientific) following the manufacturer's protocol. For immunoblotting, mAi9 cells in a 6-well plate were lysed with 1xRIPA buffer (20 mM Tris-HCl, pH 7.5, 150 mM NaCl, 1 mM Na_2EDTA, 1 mM EGTA, 1% NP-40, 1% sodium deoxycholate, 2.5 mM sodium pyrophosphate, 1 mM β-glycerophosphate, 1 mM Na_3VO_4, 1 μg/mL leupeptin, 1 mM PMSF), protein concentration was quantified by the BCA protein assay kit (TheremoFisher), and cells were treated with 0.5 volume of 3× SDS sample buffer (187.5 mM Tris-HCl, pH 6.8, 6% SDS, 30% glycerol and 0.03% bromophenol blue, 0.125 M dithiothreitol) and heated at 97 °C or boiling for 8 min. Protein samples were separated on polyacrylamide gels and transferred to polyvinylidene difluoride (PVDF) membranes. Membranes were blocked in Tris-buffered saline (TBS, pH 7.6) containing 0.5% Tween 20 (TBST) and 5% nonfat dry milk and incubated in 5% BSA in TBST, containing rabbit polyclonal anti-SpCas9 (Cell Signaling Technology, #14697, 1:5,000) and mouse monoclonal anti-6xHis (MilliporeSigma, H1029, 1:1,000) antibodies overnight. Membranes were washed three times with TBST and incubated in TBST containing 5% milk with the corresponding IgG-horseradish peroxidase conjugate, 1:5,000 (Santa Cruz Biotechnology and Cell Signaling Technology) for 1 h. After three TBST washes, peroxidase activity was revealed by enhanced chemiluminescence using ECL or ECL2 Western blotting substrate (both from Thermo Scientific) and imaged using a Chemidoc XRS imaging system (Bio-Rad Laboratories, Hercules, CA).

Conjugation of SpT and SpC. To conjugate SpT maltose-binding protein fusion protein with SpC, the two components at amounts designated in each figure were incubated in a standard phosphate-buffered saline (PBS) buffer at 21 or 37 °C for 1−2 h before the reaction content was subject to protein composition analysis by SDS-PAGE. To conjugate SpT-incorporated adenoviruses

https://doi.org/10.1021/acsnano.2c00909
ACS Nano 2022, 16, 10443−10455

with SpC or with Cas9SpC/gRNA, viruses and SpC or Cas9SpC were incubated in PBS containing 10% glycerol at 21 or 37 °C for 2 h. Lox sgRNA at designated amounts was added to the reaction content, and the mixture was incubated at 21 °C for 10−15 min before application to cell culture medium or subject to protein composition analysis by SDS-PAGE.

CRISPR-Cas9 Gene-Editing Assay with mAi9 and A549 Cells. For lipofectamine CRISPRMAX transfection of mAi9 cells, 1.0×10^5 cells were seeded in individual wells of a 24-well plate, and 16 h later, the cells were transfected using Lipofectamine CRISPRMAX according to the manufacturer's protocol. The amounts of TrueCut Cas9 v2 or Cas9SpC and lox gRNA are designated in Figure 1. For adenovirus transduction of mAi9 and A549 cells, 0.5×10^4 to 2.0×10^5 cells (designated in each experiment) were seeded in individual wells of a 24-well plate, and 18 h later, the cell culture was replaced with fresh medium containing various amounts of viruses premixed with or without 7.5 pmol of Cas9SpC/gRNA. CRISPR-Cas9 gene-editing analyses were carried out in mAi9 cell cultures 4 days post transfection or virus transduction and in A549 cells 48 h post virus infection.

Immunofluorescence, Fluorescence Microscopy, and Flow Cytometry Analysis. For immunofluorescence staining, 2×10^4 mAi9 cells were seeded in Nunc Lab-Tek II 8-well chamber slides (ThermoFisher) and, 16 h later, were infected with SpT viruses conjugated with Cas9SpC/tdT gRNA, fixed in 4% paraformaldehyde for 30 min and then at 4 °C in protein block (5% donkey serum in PBS) containing primary antibodies overnight or longer. Primary antibodies used in this study included mouse anti-SpCas9 (Cell Signaling Technology, #14697, 1:400) and goat anti-Ad5 hexon. On day 2, the slides were washed three times in PBS, incubated with corresponding 1:400 diluted Alexa Fluor594- and Fluor647-conjugated secondary antibodies (Jackson ImmunoResearch Laboratories), and counterstained with SlowFade Gold Antifade mounting reagent with 4,6-diamidino-2 phenylindole (DAPI) (Thermo Fisher Scientific). White-light, fluorescence, and immunofluorescence microscope images were collected using an Olympus DP71 color microscope digital camera (Olympus America). The optimized camera acquisition time for tdTomato fluorescence was set *a priori* using cells without tdTomato expression in each experiment. The percentage of tdTomato-positive areas was quantified with CellSens Dimension imaging software (Olympus). A threshold defining the background signal intensity was set using micrographs collected from untreated mAi9 cells, and pixels with above the background red color intensity were identified and summed. The percentage of tdTomato-positive area to total micrograph area was calculated. The tdTomato expression in mAi9 cells was also analyzed by flow cytometry. Adherent mAi9 cells were detached into a single cell suspension by trypsin/EDTA and analyzed directly without fixation by an Attune NxT flow cytometer using a YL-1 laser (ThermoFisher).

Genomic DNA PCR and Sequencing Analysis of mAi9 *Rosa26-tdTomato* and Human CDK4 Loci. Adherent mAi9 and A549 cells in individual wells of a 24-well plate were covered with 0.5 mL of lysis buffer (100 mM Tris-HCl, pH 8.5, 0.2% SDS, 5 mM EDTA, 200 mM NaCl, and 100 ug/mL proteinase K) and incubated at 55 °C for 4 h. The cell lysates were extracted once with equal volumes of phenol/chloroform/iso-amyl alcohol, pH 8.0, and then with chloroform, and DNA was precipitated with ethanol in the presence of sodium acetate. Dual-gene editing at the *ROSA26-tdTomato* locus was detected by PCR amplification of a fragment spanning the two loxP sites with the upper stream primer 5′-GCAACGTGCTGGTTATTGTG-3′ and downstream primer 5′-CTCACCATGGTGGCGGGATC-3′. PCR amplification yielded a 1137 bp fragment for the unedited sequence and approximately averaged truncated 194 bp fragments from the dual-edited allele with STOP cassette deletion. The truncated DNA bands were retrieved and submitted for next-generation sequencing by Genome Engineering & iPSC Center of Washington University School of Medicine. The human *CDK4* exon region was amplified by PCR using the upper stream primer 5′-GCCGGCCCCAAGGAAGACTGGGAG-3′ and downstream primer 5′-GCACAGACGTCCATCAGCC-3′. The non-truncated at ROSA26-tdTomato and CDK4 DNA bands were subject to Sanger sequencing. The inference of CRISPR editing (ICE) analysis, which is superior to TIDE analysis, was performed using the ICE calculator tool developed by the genome engineering company Synthego.[39]

ASSOCIATED CONTENT

Supporting Information

The Supporting Information is available free of charge at https://pubs.acs.org/doi/10.1021/acsnano.2c00909.

Materials and methods for the experiments shown in the supplemental figures: (1) transmission electron microcopy analysis of adenovirus vectors; (2) *in vitro* Cas9 DNA cleavage assay. Figure 1. The conjugation reaction of SpC and SpT was spontaneous and occurred in a titratable fashion. Figure 2. Cas9SpC fusion protein retained CRISPR nuclease activity. Figure 3. Diagrams showing placement of SpT on SAd36 surface capsid proteins. Figure 4. Lack of nonspecific cross-linking of Cas9SpC to unmodified SAd36 viral proteins. Figure 5. Conjugation with Cas9SpC on SpT SAd36 capsid proteins maintained virus morphology. Figure 6. Efficient gene editing in cells infected with SpT SAd36 vectors carrying Cas9SpC/gRNA on the capsid surface. Figure 7. Characteristic SpCas9 nuclease-mediated indel patterns repaired by nonhomologous end joining at two lox gRNA sites of the Rosa26-tdTomato locus. Figure 8. Cas9SpC conjugated on the SpT SAd36 virion surface retained CRISPR nuclease activity in an *in vitro* DNA cleavage assay. (PDF)

AUTHOR INFORMATION

Corresponding Author

David T. Curiel − *Department of Radiation Oncology, Biologic Therapeutics Center, Washington University School of Medicine, St. Louis, Missouri 63110, United States;* orcid.org/0000-0003-3802-6014; Email: dcuriel@wustl.edu

Authors

Zhi Hong Lu − *Department of Radiation Oncology, Biologic Therapeutics Center, Washington University School of Medicine, St. Louis, Missouri 63110, United States;* orcid.org/0000-0002-0357-8137

Jie Li − *Department of Radiation Oncology, Biologic Therapeutics Center, Washington University School of Medicine, St. Louis, Missouri 63110, United States*

Igor P. Dmitriev − *Department of Radiation Oncology, Biologic Therapeutics Center, Washington University School of Medicine, St. Louis, Missouri 63110, United States*

Elena A. Kashentseva − *Department of Radiation Oncology, Biologic Therapeutics Center, Washington University School of Medicine, St. Louis, Missouri 63110, United States*

Complete contact information is available at: https://pubs.acs.org/10.1021/acsnano.2c00909

Notes

The authors declare no competing financial interest.

ACKNOWLEDGMENTS

This work was funded by NIH UG3 TR002851 and R01 CA211096 grants to D. Curiel and by contract agreement GR0022068 with Walking Fish Therapeutics to Z. Lu. We

thank scientists from SpyBiotech Limited for sharing and discussing unpublished results related to adenovirus engineering with tags and catchers' technology. We thank Amanda Baker for providing professional drawings for adenoviral engineering schematic diagrams.

REFERENCES

(1) Mohanraju, P.; Saha, C.; van Baarlen, P.; Louwen, R.; Staals, R. H. J.; van der Oost, J. Alternative functions of CRISPR-Cas systems in the evolutionary arms race. *Nat. Rev. Microbiol.* **2022**, *20*, 351.

(2) Nidhi, S.; Anand, U.; Oleksak, P.; Tripathi, P.; Lal, J. A.; Thomas, G.; Kuca, K.; Tripathi, V. Novel CRISPR-Cas Systems: An Updated Review of the Current Achievements, Applications, and Future Research Perspectives. *Int. J. Mol. Sci.* **2021**, *22* (7), 3327.

(3) Gillmore, J. D.; Gane, E.; Taubel, J.; Kao, J.; Fontana, M.; Maitland, M. L.; Seitzer, J.; O'Connell, D.; Walsh, K. R.; Wood, K.; Phillips, J.; Xu, Y.; Amaral, A.; Boyd, A. P.; Cehelsky, J. E.; McKee, M. D.; Schiermeier, A.; Harari, O.; Murphy, A.; Kyratsous, C. A.; Zambrowicz, B.; Soltys, R.; Gutstein, D. E.; Leonard, J.; Sepp-Lorenzino, L.; Lebwohl, D. CRISPR-Cas9 In Vivo Gene Editing for Transthyretin Amyloidosis. *N Engl J. Med.* **2021**, *385* (6), 493−502.

(4) Saha, K.; Sontheimer, E. J.; Brooks, P. J.; Dwinell, M. R.; Gersbach, C. A.; Liu, D. R.; Murray, S. A.; Tsai, S. Q.; Wilson, R. C.; Anderson, D. G.; Asokan, A.; Banfield, J. F.; Bankiewicz, K. S.; Bao, G.; Bulte, J. W. M.; Bursac, N.; Campbell, J. M.; Carlson, D. F.; Chaikof, E. L.; Chen, Z. Y.; Cheng, R. H.; Clark, K. J.; Curiel, D. T.; Dahlman, J. E.; Deverman, B. E.; Dickinson, M. E.; Doudna, J. A.; Ekker, S. C.; Emborg, M. E.; Feng, G.; Freedman, B. S.; Gamm, D. M.; Gao, G.; Ghiran, I. C.; Glazer, P. M.; Gong, S.; Heaney, J. D.; Hennebold, J. D.; Hinson, J. T.; Khvorova, A.; Kiani, S.; Lagor, W. R.; Lam, K. S.; Leong, K. W.; Levine, J. E.; Lewis, J. A.; Lutz, C. M.; Ly, D. H.; Maragh, S.; McCray, P. B., Jr.; McDevitt, T. C.; Mirochnitchenko, O.; Morizane, R.; Murthy, N.; Prather, R. S.; Ronald, J. A.; Roy, S.; Roy, S.; Sabbisetti, V.; Saltzman, W. M.; Santangelo, P. J.; Segal, D. J.; Shimoyama, M.; Skala, M. C.; Tarantal, A. F.; Tilton, J. C.; Truskey, G. A.; Vandsburger, M.; Watts, J. K.; Wells, K. D.; Wolfe, S. A.; Xu, Q.; Xue, W.; Yi, G.; Zhou, J.; Consortium, S.. The NIH Somatic Cell Genome Editing program. *Nature* **2021**, *592* (7853), 195−204.

(5) Luthra, R.; Kaur, S.; Bhandari, K. Applications of CRISPR as a potential therapeutic. *Life Sci.* **2021**, *284*, 119908.

(6) Li, L.; Hu, S.; Chen, X. Non-viral delivery systems for CRISPR/Cas9-based genome editing: Challenges and opportunities. *Biomaterials* **2018**, *171*, 207−218.

(7) Lino, C. A.; Harper, J. C.; Carney, J. P.; Timlin, J. A. Delivering CRISPR: a review of the challenges and approaches. *Drug Deliv* **2018**, *25* (1), 1234−1257.

(8) Xu, C. L.; Ruan, M. Z. C.; Mahajan, V. B.; Tsang, S. H. Viral Delivery Systems for CRISPR. *Viruses* **2019**, *11* (1), 28.

(9) Hanlon, K. S.; Kleinstiver, B. P.; Garcia, S. P.; Zaborowski, M. P.; Volak, A.; Spirig, S. E.; Muller, A.; Sousa, A. A.; Tsai, S. Q.; Bengtsson, N. E.; Loov, C.; Ingelsson, M.; Chamberlain, J. S.; Corey, D. P.; Aryee, M. J.; Joung, J. K.; Breakefield, X. O.; Maguire, C. A.; Gyorgy, B. High levels of AAV vector integration into CRISPR-induced DNA breaks. *Nat. Commun.* **2019**, *10* (1), 4439.

(10) Yip, B. H. Recent Advances in CRISPR/Cas9 Delivery Strategies. *Biomolecules* **2020**, *10* (6), 839−855.

(11) Mehta, A.; Merkel, O. M. Immunogenicity of Cas9 Protein. *J. Pharm. Sci.* **2020**, *109* (1), 62−67.

(12) Paunovska, K.; Loughrey, D.; Dahlman, J. E. Drug delivery systems for RNA therapeutics. *Nat. Rev. Genet* **2022**, *23*, 265−280.

(13) Gomez-Aguado, I.; Rodriguez-Castejon, J.; Vicente-Pascual, M.; Rodriguez-Gascon, A.; Solinis, M. A.; Del Pozo-Rodriguez, A. Nanomedicines to Deliver mRNA: State of the Art and Future Perspectives. *Nanomaterials (Basel)* **2020**, *10* (2), 364−406.

(14) Mu, X.; Hur, S. Immunogenicity of In Vitro-Transcribed RNA. *Acc. Chem. Res.* **2021**, *54* (21), 4012−4023.

(15) Zhang, S.; Shen, J.; Li, D.; Cheng, Y. Strategies in the delivery of Cas9 ribonucleoprotein for CRISPR/Cas9 genome editing. *Theranostics* **2021**, *11* (2), 614−648.

(16) Duan, L.; Ouyang, K.; Xu, X.; Xu, L.; Wen, C.; Zhou, X.; Qin, Z.; Xu, Z.; Sun, W.; Liang, Y. Nanoparticle Delivery of CRISPR/Cas9 for Genome Editing. *Front Genet* **2021**, *12*, 673286.

(17) Zuris, J. A.; Thompson, D. B.; Shu, Y.; Guilinger, J. P.; Bessen, J. L.; Hu, J. H.; Maeder, M. L.; Joung, J. K.; Chen, Z. Y.; Liu, D. R. Cationic lipid-mediated delivery of proteins enables efficient protein-based genome editing in vitro and in vivo. *Nat. Biotechnol.* **2015**, *33* (1), 73−80.

(18) Staahl, B. T.; Benekareddy, M.; Coulon-Bainier, C.; Banfal, A. A.; Floor, S. N.; Sabo, J. K.; Urnes, C.; Munares, G. A.; Ghosh, A.; Doudna, J. A. Efficient genome editing in the mouse brain by local delivery of engineered Cas9 ribonucleoprotein complexes. *Nat. Biotechnol.* **2017**, *35* (5), 431−434.

(19) Chen, G.; Abdeen, A. A.; Wang, Y.; Shahi, P. K.; Robertson, S.; Xie, R.; Suzuki, M.; Pattnaik, B. R.; Saha, K.; Gong, S. A biodegradable nanocapsule delivers a Cas9 ribonucleoprotein complex for in vivo genome editing. *Nat. Nanotechnol* **2019**, *14* (10), 974−980.

(20) Evans, B. C.; Fletcher, R. B.; Kilchrist, K. V.; Dailing, E. A.; Mukalel, A. J.; Colazo, J. M.; Oliver, M.; Cheung-Flynn, J.; Brophy, C. M.; Tierney, J. W.; Isenberg, J. S.; Hankenson, K. D.; Ghimire, K.; Lander, C.; Gersbach, C. A.; Duvall, C. L. An anionic, endosome-escaping polymer to potentiate intracellular delivery of cationic peptides, biomacromolecules, and nanoparticles. *Nat. Commun.* **2019**, *10* (1), 5012.

(21) Wei, T.; Cheng, Q.; Min, Y. L.; Olson, E. N.; Siegwart, D. J. Systemic nanoparticle delivery of CRISPR-Cas9 ribonucleoproteins for effective tissue specific genome editing. *Nat. Commun.* **2020**, *11* (1), 3232.

(22) Banskota, S.; Raguram, A.; Suh, S.; Du, S. W.; Davis, J. R.; Choi, E. H.; Wang, X.; Nielsen, S. C.; Newby, G. A.; Randolph, P. B.; Osborn, M. J.; Musunuru, K.; Palczewski, K.; Liu, D. R. Engineered virus-like particles for efficient in vivo delivery of therapeutic proteins. *Cell* **2022**, *185* (2), 250−265.

(23) Lee, C. S.; Bishop, E. S.; Zhang, R.; Yu, X.; Farina, E. M.; Yan, S.; Zhao, C.; Zeng, Z.; Shu, Y.; Wu, X.; Lei, J.; Li, Y.; Zhang, W.; Yang, C.; Wu, K.; Wu, Y.; Ho, S.; Athiviraham, A.; Lee, M. J.; Wolf, J. M.; Reid, R. R.; He, T. C. Adenovirus-Mediated Gene Delivery: Potential Applications for Gene and Cell-Based Therapies in the New Era of Personalized Medicine. *Genes Dis.* **2017**, *4* (2), 43−63.

(24) Dmitriev, I. P.; Kaliberov, S. A. Targeted Adenoviral Vectors I: Transductional Targeting. In *Adenoviral Vectors for Gene Therapy*, 2nd ed.; Curiel, D. T., Ed.; Elsevier: Cambridge, MA, 2016; pp 231−257.

(25) Luisoni, S.; Greber, U. F. Biology of adenovirus cell entry: receptors, pathways, mechanisms. In *Adenoviral vectors for gene therapy*, 2nd ed.; Curiel, D. T., Ed.; Elsevier: Cambridge, MA, 2016; pp 27−58.

(26) Greber, U. F.; Gomez-Gonzalez, A. Adenovirus - a blueprint for gene delivery. *Curr. Opin Virol* **2021**, *48*, 49−56.

(27) Suomalainen, M.; Luisoni, S.; Boucke, K.; Bianchi, S.; Engel, D. A.; Greber, U. F. A direct and versatile assay measuring membrane penetration of adenovirus in single cells. *J. Virol* **2013**, *87* (22), 12367−79.

(28) Pied, N.; Wodrich, H. Imaging the adenovirus infection cycle. *FEBS Lett.* **2019**, *593* (24), 3419−3448.

(29) Curiel, D. T.; Agarwal, S.; Wagner, E.; Cotten, M. Adenovirus enhancement of transferrin-polylysine-mediated gene delivery. *Proc. Natl. Acad. Sci. U. S. A.* **1991**, *88* (19), 8850−4.

(30) Curiel, D. T.; Wagner, E.; Cotten, M.; Birnstiel, M. L.; Agarwal, S.; Li, C. M.; Loechel, S.; Hu, P. C. High-efficiency gene transfer mediated by adenovirus coupled to DNA-polylysine complexes. *Hum. Gene Ther.* **1992**, *3* (2), 147−54.

(31) Keeble, A. H.; Turkki, P.; Stokes, S.; Khairil Anuar, I. N. A.; Rahikainen, R.; Hytonen, V. P.; Howarth, M. Approaching infinite affinity through engineering of peptide-protein interaction. *Proc. Natl. Acad. Sci. U. S. A.* **2019**, *116* (52), 26523−26533.

https://doi.org/10.1021/acsnano.2c00909
ACS Nano 2022, 16, 10443−10455

(32) Wu, Y.; Zeng, J.; Roscoe, B. P.; Liu, P.; Yao, Q.; Lazzarotto, C. R.; Clement, K.; Cole, M. A.; Luk, K.; Baricordi, C.; Shen, A. H.; Ren, C.; Esrick, E. B.; Manis, J. P.; Dorfman, D. M.; Williams, D. A.; Biffi, A.; Brugnara, C.; Biasco, L.; Brendel, C.; Pinello, L.; Tsai, S. Q.; Wolfe, S. A.; Bauer, D. E. Highly efficient therapeutic gene editing of human hematopoietic stem cells. *Nat. Med.* **2019**, *25* (5), 776−783.
(33) Roy, S.; Medina-Jaszek, A.; Wilson, M. J.; Sandhu, A.; Calcedo, R.; Lin, J.; Wilson, J. M. Creation of a panel of vectors based on ape adenovirus isolates. *J. Gene Med.* **2011**, *13* (1), 17−25.
(34) Fonseca, J. A.; McCaffery, J. N.; Kashentseva, E.; Singh, B.; Dmitriev, I. P.; Curiel, D. T.; Moreno, A. A prime-boost immunization regimen based on a simian adenovirus 36 vectored multi-stage malaria vaccine induces protective immunity in mice. *Vaccine* **2017**, *35* (24), 3239−3248.
(35) Hassan, A. O.; Kafai, N. M.; Dmitriev, I. P.; Fox, J. M.; Smith, B. K.; Harvey, I. B.; Chen, R. E.; Winkler, E. S.; Wessel, A. W.; Case, J. B.; Kashentseva, E.; McCune, B. T.; Bailey, A. L.; Zhao, H.; VanBlargan, L. A.; Dai, Y. N.; Ma, M.; Adams, L. J.; Shrihari, S.; Danis, J. E.; Gralinski, L. E.; Hou, Y. J.; Schafer, A.; Kim, A. S.; Keeler, S. P.; Weiskopf, D.; Baric, R. S.; Holtzman, M. J.; Fremont, D. H.; Curiel, D. T.; Diamond, M. S. A Single-Dose Intranasal ChAd Vaccine Protects Upper and Lower Respiratory Tracts against SARS-CoV-2. *Cell* **2020**, *183* (1), 169−184.
(36) Hassan, A. O.; Feldmann, F.; Zhao, H.; Curiel, D. T.; Okumura, A.; Tang-Huau, T. L.; Case, J. B.; Meade-White, K.; Callison, J.; Chen, R. E.; Lovaglio, J.; Hanley, P. W.; Scott, D. P.; Fremont, D. H.; Feldmann, H.; Diamond, M. S. A single intranasal dose of chimpanzee adenovirus-vectored vaccine protects against SARS-CoV-2 infection in rhesus macaques. *Cell Rep. Med.* **2021**, *2* (4), 100230.
(37) Morris, S. J.; Sebastian, S.; Spencer, A. J.; Gilbert, S. C. Simian adenoviruses as vaccine vectors. *Future Virol* **2016**, *11* (9), 649−659.
(38) Krasnykh, V.; Belousova, N.; Korokhov, N.; Mikheeva, G.; Curiel, D. T. Genetic targeting of an adenovirus vector via replacement of the fiber protein with the phage T4 fibritin. *J. Virol* **2001**, *75* (9), 4176−83.
(39) Conant, D.; Hsiau, T.; Rossi, N.; Oki, J.; Maures, T.; Waite, K.; Yang, J.; Joshi, S.; Kelso, R.; Holden, K.; Enzmann, B. L.; Stoner, R. Inference of CRISPR Edits from Sanger Trace Data. *CRISPR J.* **2022**, *5* (1), 123−130.
(40) Goswami, R.; Subramanian, G.; Silayeva, L.; Newkirk, I.; Doctor, D.; Chawla, K.; Chattopadhyay, S.; Chandra, D.; Chilukuri, N.; Betapudi, V. Gene Therapy Leaves a Vicious Cycle. *Front Oncol* **2019**, *9*, 297−322.
(41) Greber, U. F.; Webster, P.; Weber, J.; Helenius, A. The role of the adenovirus protease on virus entry into cells. *EMBO J.* **1996**, *15* (8), 1766−77.
(42) Takahashi, E.; Cohen, S. L.; Tsai, P. K.; Sweeney, J. A. Quantitation of adenovirus type 5 empty capsids. *Anal. Biochem.* **2006**, *349* (2), 208−17.
(43) Ahi, Y. S.; Mittal, S. K. Components of Adenovirus Genome Packaging. *Front Microbiol* **2016**, *7*, 1503−1518.

https://doi.org/10.1021/acsnano.2c00909
ACS Nano 2022, 16, 10443−10455